Dean&Francis
ISSN 2959-6157

# Coronal Mass Ejections modelling simulation

**Jiayi Liu**

High School Affliated to Nanjing Normal University, Nanjing, 210003, China

jiayiliuhorn@outlook.com

**Abstract:**

A violent solar eruption has the potential to disrupt the normal functioning of radio and cell phone technology, impeding communication and navigation. In addition, it could cause direct damage to artificial vehicles, resulting in non-structrual effects on the current human environment. In this paper, a solar eruption event was selected to represent typical occurrences, encompassing both solar flares and a coronal mass ejection. According to multiband observations, the flare is triggered by the magnetic flow emerging and disturbing the quadrupole magnetic field structure. The far-UV band observations found that the flare burst caused significant far-UV waves. We analyze the temporality of flare and coronal mass ejections to determine coronal mass ejections and flare are two manifestations of the same eruption event. This research adopted an improved cone model according to the multi-angle observation to simulate the real propagation direction, velocity and morphological evolution after the eruption, aimed to give an early warning to the earth's space environment.

**Key** words: solar flares; coronal mass ejection; cone model

## 1 Introduction

Life on Earth cannot exist without light energy from the sun's radiation[2-4]. The Sun is the closest and most influential star to the Earth in the universe, the average Geodetic Distance from the Sun to the Earth is 150 million kilometers. High-resolution observations of the Sun allow us to study detailed changes on the solar surface. In solar-terrestrial space, solar activity may have a serious impact on or even jeopardize the human living environment. Solar activity occurs on the Sun, and violent solar activity is sometimes referred to as solar eruptions[3]. These include solar eruptions, solar flare eruptions, and coronal mass ejections. They are all essentially the result of the release of magnetic energy after a certain stage in the evolution of the Sun's magnetic field. As the magnetic field undergoes a variety of transformations, researchers are able to observe a range of phenomena[5]. A Solar flare is a cold and dense plasma in the solar atmosphere, situated above the photosphere. It has a temperature of approximately 0.1% of the corona and a density of approximately 100 times that of the corona. The energy released by a normal flare is up to

ISSN 2959-6157

$10^{32}$erg ($10^{25}$ J) [5,6]. It is one of the most common features of the solar atmosphere. Flares can be observed in the Hα-band, CallH-band, ultraviolet and extreme ultraviolet bands, which are observed as colder and denser objects than their surroundings. A sunburst located on the edge of the sun's surface and represented as a bright prominence is referred to as a flare or Helios. Similarly, a sunburst located on the sun's surface and represented as a bar that is darker than its surroundings is also classified as a flare. However, if the bar is observed to be darker than the surrounding area, it is designated as a dark bar. It can be argued that flares/dark bars are essentially the same type of feature[7]. The analysis of flares by scientific observers has demonstrated that they are constituted of intricate fibrous structures, with fibers that are subject to a considerable degree of motion dynamics. The fibers can be divided into two main categories based on their orientation: transverse, running parallel to the axial direction, and vertical, running perpendicular to the axial direction.

The study of white flares has been conducted for over a century and a half, beginning with the initial discovery in 1859. The classification of flares can be approached from a variety of perspectives[11]. The International Astronomical Union (IAU) has established a standard for measuring the intensity of soft X-ray flows, with values ranging from A to X. This standard is used to categorize flares as weak (A), moderate (B), strong (C), very strong (M), and extreme (X). Additionally, the increasing flow rate is indicative of the corresponding increase in energy. The evolution of a flare can be divided into three stages, based on its characteristics: prophase, pulse phase, and attenuation phase. The morphological characteristics of flares (chiefly those observable in the chromosphere) can be classified into two principal categories: dense flares and double-band flares. It is typical for large flares to manifest as double-band flares. A new theory posits that, with higher-resolution observations, dense flares may also consist of multiple bright bands, which would be double-band flares.

Coronal mass ejections (CME) are the most frequent and spectacular large-scale activity phenomenon in the solar atmosphere. The discovery of CMEs led to the rapid realization that fluctuations in the Earth's magnetic field are frequently strongly associated with the occurrence of CMEs[8]. The phenomenon of sudden and instantaneous ejection of matter was first observed in the early 1970s by the White Light Coronagraph on board the US Naval Laboratory's OSO-7 satellite[8]. In particular, the coronagraph LASCO, which was launched by the SOHO satellite at the end of 1995, observed a significant number of CME. The STEREO satellite, which was launched in 2006, carried the coronagraph and provided multi-angle observation, as well as cooperating with the Earth perspective to form a three-dimensional observation of CME[12]. This has contributed to a greater understanding of CME.

The traditional CME standard flare model (CSHKP) is capable of simultaneously explaining a multitude of phenomena associated with the outburst process, including pulse acceleration, flare band separation, and post-flare ring rise[9]. The trigger model of CME primarily elucidates the genesis of the primary energy release. The model is classified into two categories: the magnetic reconnection trigger model and the ideal trigger model. While the physical properties of the individual structures and the coronal dark regions have been revealed to some extent in previous studies, detailed density and temperature information remains scarce. Recently, differential radiometry has also been employed to diagnose the physical parameters of CMEs[10]. Spectroscopic observations have revealed the DEM curves of bright nuclei, indicating a slight increase in temperature during the ejection process.

In this work, a solar flare and CME event were analyzed utilizing multi-angle observations. We adopted an improved cone model, incorporating data from the SOHO, STEREO, and SDO satellites, to simulate the propagation, velocity, and morphological evolution of the CME. This study presents a comprehensive analysis of the ejection conditions, temperature-density properties, and kinematic evolution of CMEs, along with a detailed examination of the physical properties of the associated waves. The review offered a significant advancement in our understanding of the origin, structure, and evolution of CMEs. And aim of this research is to improve the prediction of CME impacts on Earth's space weather environment and provide early warnings to minimize potential damage.

2.Theory

## 2.1 Standard modelling of CME

A typical double-band flare is shown in Figure 1 below. The double-band flare generally has two or more bright bands, and these bright bands are located in the opposite polar magnetic field region on either side of the magnet-neutral line. Considering the observational characteristics of two-band flares, astronomers have proposed a classical CSHKP two-dimensional flare model based on magnetic reconnection (as in Figure 2). The magnetic rope (or dark bar) initially above the magnetic neutral line is bound by the magnetic field covering it. Due to the emergence of magnetic flow and other reasons, the stability of the overall structure, results in the magnetic rope (or dark bar) lifting upward, while the covered magnetic field is stretched upward. This process leads to the "leg" covering the magnetic field under the magnetic rope, where the opposite polar magnetic lines converge to each other and eventually reconnect, releasing magnetic energy.

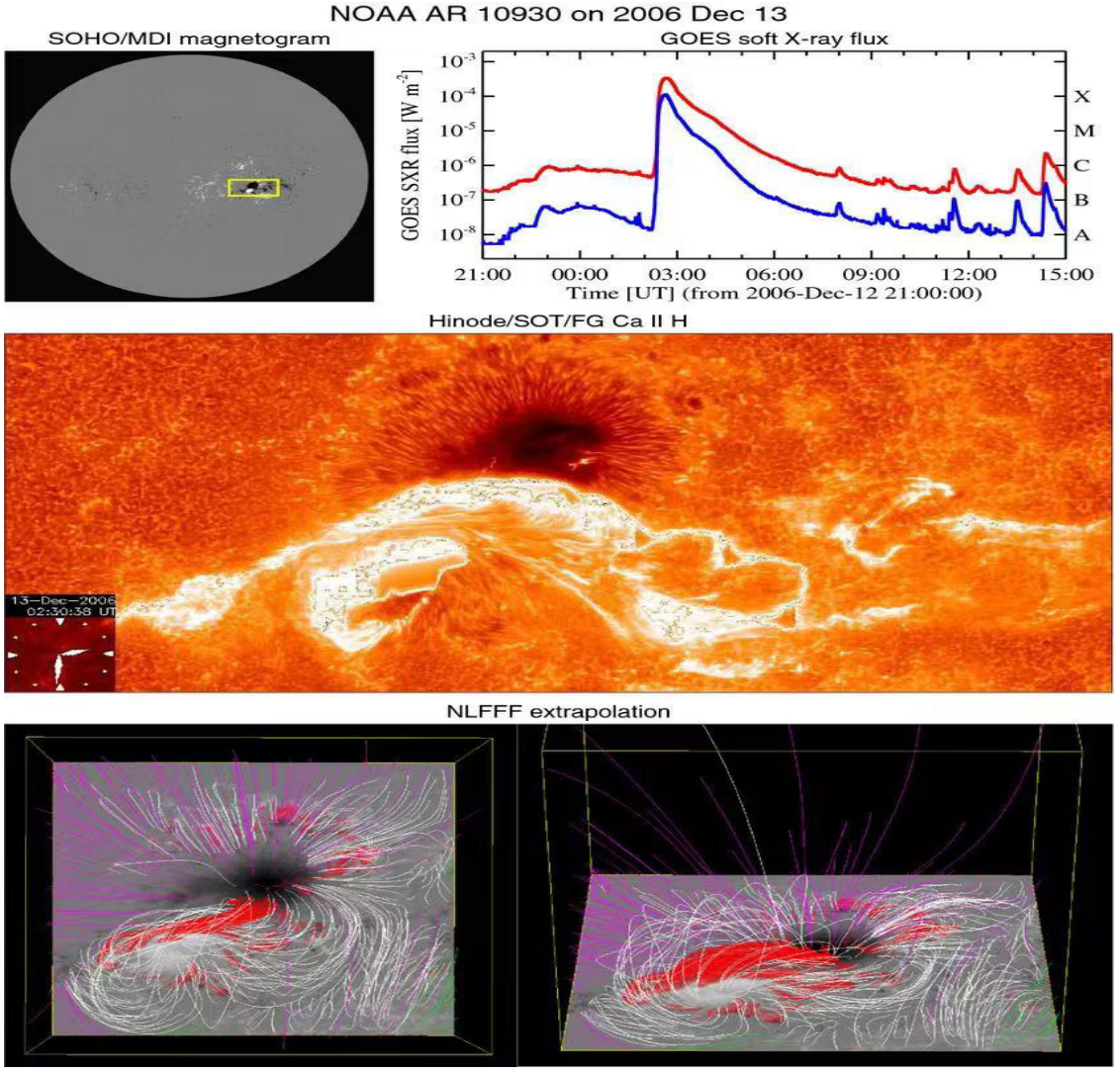


**Figure 1. The upper left is the full daily magnetic map taken by SOHO/MDI, and the upper right is the flow changes of two soft X-ray bands of GOES. The observed flare can be graded to X3.4. The following figure is the Ca II H band of Hinode/SOT/FG of an X3.4 large flare in the NOAA10930 active area (i.e. the box area on the left), showing the flare double band at the edge of the sunspot.**

ISSN 2959-6157

Part of the released magnetic energy is converted into an almost full band of electromagnetic radiation, which also accelerates the plasma in the reconnection zone, forming a high-energy high- speed outflow moving up and down along the magnetic line. The downward outflow shocks the lower atmosphere along the magnetic line and transfers energy to the plasma along the way, forming a flare double band. At the same time, high-energy electrons will collide with the high-density plasma in the low atmosphere, generating hard X-ray (foot) sources through bremsstrahlung radiation. The heated chromospheric plasma located at the flared foot is "evaporated" up the magnetic line. Chromosphere evaporation brings a large amount of high-temperature and high-density plasma to the flare ring, mainly forming ring structures with tips in the far-ultraviolet and soft X-ray bands. With the continuous rise of the magnetic rope (or dark bar), more and more magnetic lines participate in reconnection, and the reconnection position is getting higher and higher, the observed flare double band will gradually separate, and the pointed flare ring will gradually expand.

If the magnetic rope can continue to lift upward and eventually break free from the sun, carrying a large number of high-energy plasmas, the sun's magnetic field will enter interplanetary space to form the CME.

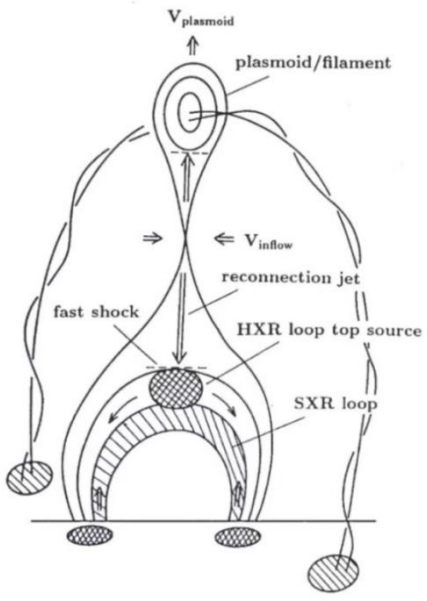


**Figure 2. CSHKP model of classical solar flare**

Although CME affects Earth dramatically, not all CME can hit Earth. As shown in Figure 3, the solar interplanetary magnetic field is a spiral structure due to solar rotation. CME travels along the interplanetary space, causing CME from the Sun opposite the eastern hemisphere of the Earth's face to reach Earth, while CME in the western hemisphere hit Earth. It takes time for CME to reach Earth. Assuming that CME is linear in the interstellar propagation, the average burst velocity of CME is about 1000km/s, and the average daily-ground distance is about $1.5\times10^8$ km, so the transmission time is about 1.74days. Since the actual motion of CME in interplanetary space is an arc, it generally takes $2-3$days for CME to reach Earth. Thus providing a warning time to reduce the impact of solar flare outbreaks on human survival. If a violent coronal mass ejection on the earth, it may hit the earth more than ten hours later. This is rare, such as the giant solar storm of 1859. If there is only one perspective observation, the projection effect is difficult to accurately judge the parameters of CME. The current CME cone model is a 3D simulation based on a single perspective of the SOHO satellite. Due to the occlusion, the outbreak source area of CME cannot be determined, so the azimuth angle cannot accurately be judged, resulting in the rough accuracy and accuracy of the simulation. The comprehensive use of multi-band multi-perspective observation and the improved 3D simulation of the cone model is conducive to the 3D reconstruction of CME, and the more accurate prediction of propagation direction and velocity, to provide reference for the warning of earth's space weather warning.

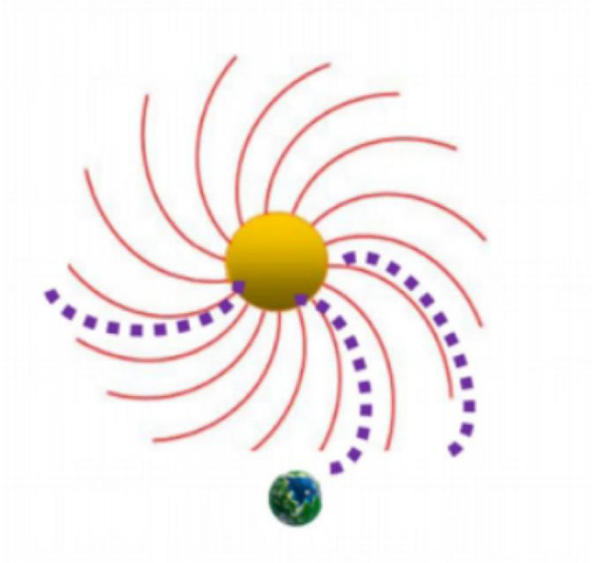

**Figure 3. Schematic diagram of the spiral structure of the solar interplanetary magnetic field**

CME represents a large-scale structure, comprising a substantial quantity of plasma propelled from the solar corona and a robust solar magnetic field into interplanetary space. The total mass of material ejected by a CME burst is typically in the range of $10^{11}$-$10^{12}$ kg, with an overall ejection speed of 400-1,000 km/s. In rare instances, this speed can

reach several thousand kilometers per second. A CME impact on Earth will result in geomagnetic storms and the destruction of the Earth's ionospheric ozone layer, thereby inflicting significant damage to the modern, high-tech society that is dependent on electromagnetic technology.

CME frequently manifests in a variety of forms, including jet, ring, bubble, and halo. It is widely accepted that the observed projection effect is the primary cause of the diverse forms of CME observed in nature. As illustrated in Figure 4, a typical CME frequently exhibits a three-component structure, comprising a bright outer ring, a low-density dark cavity, and a high-density bright core. The CME bright core is a magnetic rope structure that lifts and eventually erupts, while the dark cavity becomes a low-density region. As the magnetic flux rope expands and the magnetic field around the core undergoes continuous reconnection, the volume of the dark cavity gradually decreases. The evolution of CME is similar to flare res, with an initial phase, pulse (accelerated) phase and gentle form. As the most intense explosion in the outer atmosphere of the sun, the relationship between flares and CME has always been the subject of solar physics.

However, the use of the coronagraph CME observation technique allows for the minimization of the influence of photospheric scattering light in the area between the edge and the low corona. This, in turn, has the effect of making it more difficult to accurately judge the CME outbreak source area, and even to determine whether it is on the Sun's front or back. This, in turn, has the effect of making it more difficult to accurately predict the CME jet direction, real speed, and other parameters, which in turn affects the space weather environment early warning.

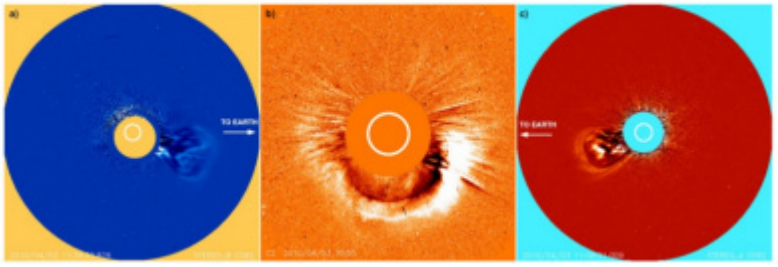

**Figure 4. Image of a coronal mass ejection from different perspectives. (a)STEREO/COR 2-B, (b)LASCO/C2 and(c) STEREO/COR 2-A were taken at almost the same time, when the STEREO satellites were between about 140.and the Earth was located on its angular bisection**

## 2.2 Standard Cone Modelling

The cone model is a simplified geometrical approach that is commonly utilized for the modeling and simulation of the propagation of coronal mass ejections (CMEs) from the Sun into interplanetary space. The model assumes that the CME expands as a self-similar cone structure, with the width and propagation speed of the cone characterized by its apex at the solar surface. The principal advantage of this model is its capacity to provide an initial approximation of CME dynamics, thereby enabling the prediction of its trajectory and impact on Earth's space weather.

In the standard cone model, the CME is considered to have a constant angular width, typically ranging between 30° and 60°, and the front of the CME is treated as an expanding spherical surface. The propagation velocity is assumed to be constant, which facilitates the computation of the CME's travel time to Earth. The model considers solely the initial propagation direction and speed, disregarding potential interactions with the surrounding solar wind and magnetic fields.

The principal computational parameters are as follows:

Cone Angle (θ): This parameter defines the angular extent of the CME. Propagation velocity (v): The speed of a CME can range from 400 to over 3000 km/s. Direction of Ejection: This is based on observations from multiple spacecraft (such as SOHO and STEREO) and determines whether the CME is Earth-directed. However, the standard cone model assumes that the CME expands uniformly, which can lead to inaccuracies, particularly for complex events where the CME may undergo significant deformation or interaction with solar wind streams. A detailed formula can be found in Figure 5.

ISSN 2959-6157

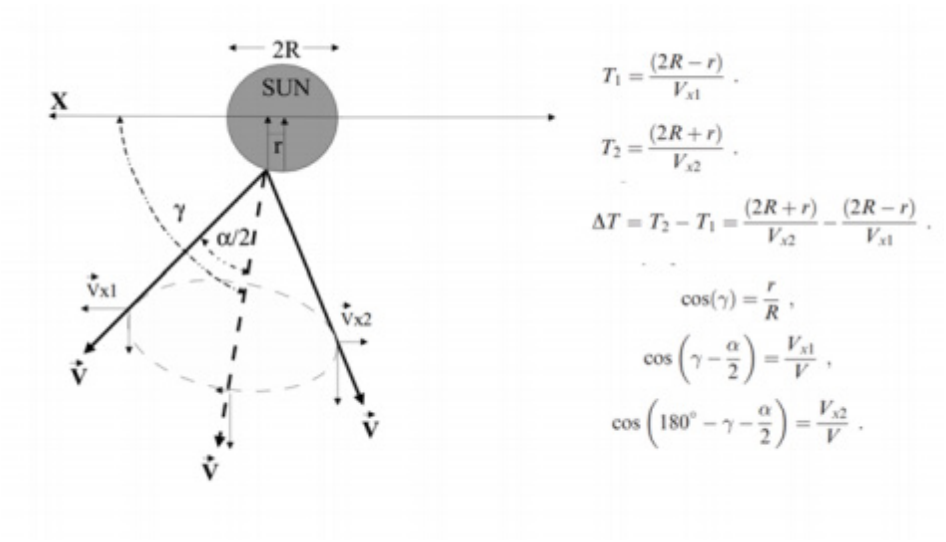


$$T_1 = \frac{(2R - r)}{V_{x1}} .$$

$$T_2 = \frac{(2R + r)}{V_{x2}} .$$

$$\Delta T = T_2 - T_1 = \frac{(2R + r)}{V_{x2}} - \frac{(2R - r)}{V_{x1}} .$$

$$\cos(\gamma) = \frac{r}{R} ,$$

$$\cos\left(\gamma - \frac{\alpha}{2}\right) = \frac{V_{x1}}{V} ,$$

$$\cos\left(180^\circ - \gamma - \frac{\alpha}{2}\right) = \frac{V_{x2}}{V} .$$

**Figure 5. Normal cone model computational formula**

## 2.3 Improved Cone Modelling

To enhance the accuracy of the standard cone model, an improved cone model was implemented. This enhanced iteration incorporates multi-angle observations from SOHO, STEREO, and SDO satellites, thereby facilitating a more comprehensive reconstruction of the CME's three-dimensional structure. Furthermore, this model modifies the propagation speed as the CME progresses, taking into account the acceleration phase that occurs during the initial eruption and the deceleration that occurs as the CME interacts with the solar wind, as shown in Figure 6.

The key features of the improved cone model are as follows:

Multi-angle observation data were incorporated into the model. The utilization of data from both Earth-based (SOHO) and off-angle (STEREO) perspectives enables a more precise estimation of the true direction and three-dimensional shape of the CME.

Variable Speed Adjustment: In contrast to the previous assumption of a constant velocity, the improved model incorporates observations of CME acceleration during the initial phase and deceleration as it propagates through the interplanetary medium.

Dynamic Expansion of the CME: The model allows for the gradual widening of the CME's angular extent based on real-time data from the instruments, thereby providing a more accurate representation of the CME's expansion as it moves away from the Sun.

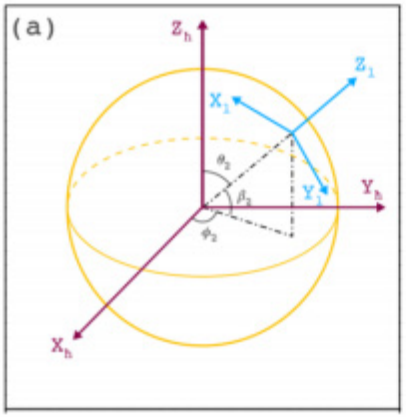


$$\begin{pmatrix} x_h \\ y_h \\ z_h \end{pmatrix} = M_2 \begin{pmatrix} x_1 \\ y_1 \\ z_1 \end{pmatrix},$$

$$M_2 = \begin{pmatrix} \cos\theta_2 \cos\phi_2 & -\sin\phi_2 & \cos\phi_2 \sin\theta_2 \\ \cos\theta_2 \sin\phi_2 & \cos\phi_2 & \sin\phi_2 \sin\theta_2 \\ -\sin\theta_2 & 0 & \cos\theta_2 \end{pmatrix}.$$

**Figure 6. Improved cone model computational formula**

# 3 Experiment

## 3.1 Event Selection

CME cases are selected exploding on the western edge of the day according to the CME event list of the SOHO satellite1.

Based on the selected CME cases and according to the SDO satellite observation data, we select the flare in the western hemisphere of the Sun which is within 1 hour before the outbreak of CME. On the basis of the first two steps, the STEREO satellite was observed from the Sun relative to the Earth.

Based on the above principles, a flare of the 17:20 UT outbreak on January 18, 2022 and a CME event observed subsequently (half an hour) were selected as the study objects.

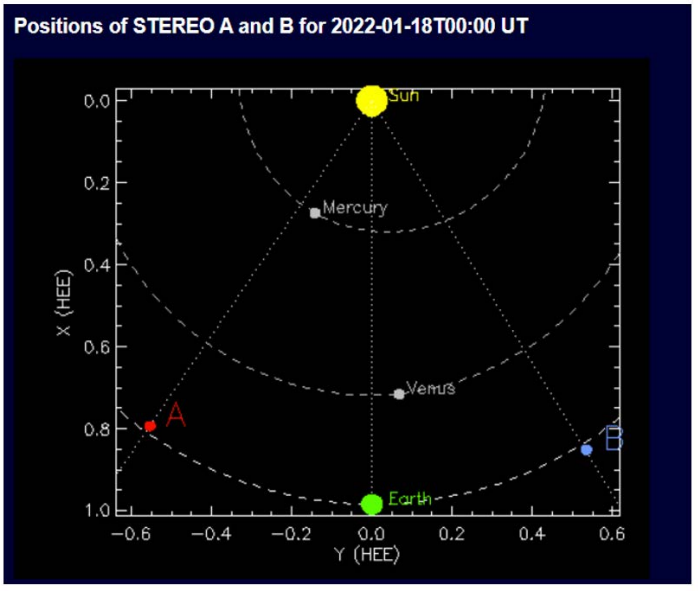


**Figure 7. Diagram of STEREO A satellite location on January 18, 2022 Data for this event from SDO and STEREO satellites were downloaded and collected.**

## 3.2 Data sources and processing

As demonstrated in the preceding analysis, multi-band and multi-angle observation data from the database were employed for the following purposes:

1. The AIA payload of the SDO (Solar Dynamics Observatory) satellite can provide comprehensive daily UV (ultraviolet) data with wavelengths of 1600 and 1700 A, an exposure time of 24 s, and far UV (extreme ultraviolet) data with wavelengths of 94, 131, 171, 193, 211, 304, and 335 A, and an exposure time of 12 s. All of the aforementioned data sets possess a spatial resolution of 1.5 arcseconds.

2. The HMI load of SDO3 provides comprehensive daily visual (line-of-sight: LOS) magnetic field data with an exposure time of 45 seconds and a spatial resolution of 1.

3. STEREO satellite observations of EUV data at wavelengths of 195 and 304A, with a temporal resolution of 5 minutes and a spatial resolution of 2.5 arcseconds.

4. White light coronagraphs include (1) SOHO, which carries LASCO4, including C2 and C3, and (2) SECCHI, which carries SECCHI5, including both COR 1 and COR 2. The LASCO/C2 field of view (FOV) encompasses a range of 2-6 solar radii (R), while C3 extends to 3.7-30 R. The time resolution is 10 m. COR 1 has a FOV of 1.4-4 R, and COR 2 has a FOV of 2.5-15 R. The time resolution is 15 m.

The software utilized in this study is IDL (Interactive Data Language), an interactive data language, and the SSW (Solar Software) software package.

ISSN 2959-6157

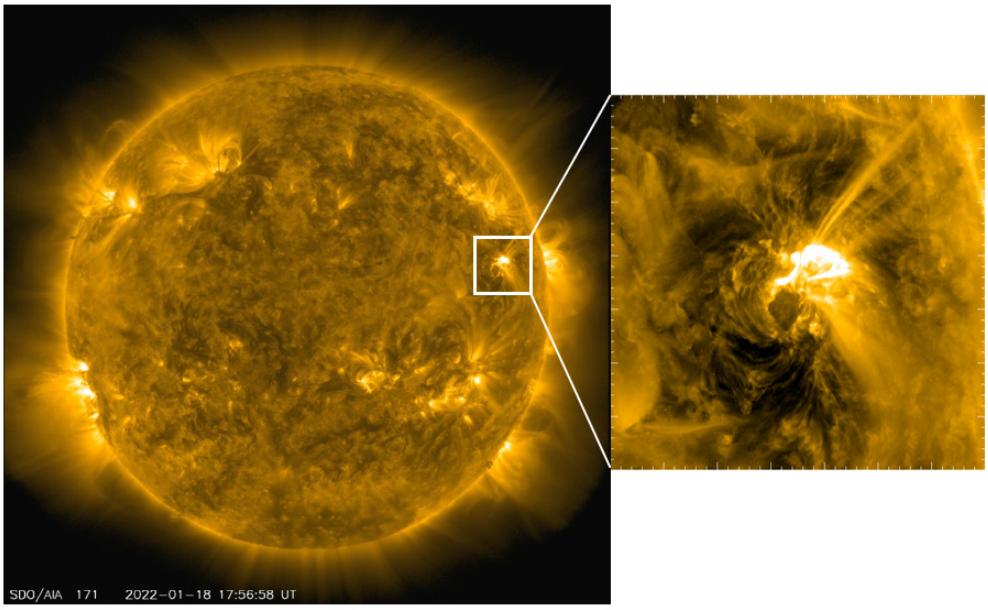


**Figure 8. Example of processing data using IDL: according to need, data of different satellites are made into video to facilitate the analysis and research.**

### 3.3 Simulation Implementation

In conducting our simulation, we employed the use of IDL (Interactive Data Language) in conjunction with the SSW (SolarSoftWare) package, which furnished us with a comprehensive framework for the effective handling and management of multi-spectral solar data. The CME data were processed from the SDO and STEREO satellites, with a particular focus on the EUV (Extreme Ultra-violet) images. Subsequently, the modified cone model was employed to reconstruct the CME's three-dimensional propagation and estimate its velocity and direction.

In this study, the enhanced cone model yielded a CME propagation speed of approximately 1409 km/s with an azimuth of 278°. The three-dimensional morphology of the CME was reconstructed by aligning the cone model output with the coronagraph images from SOHO and STEREO. This method provides a more precise estimation of the CME's trajectory, thereby facilitating more accurate predictions of potential impacts on Earth's space weather environment.

### 3.4 Data analysis

According to the GOES satellite 1-8A soft X-ray flow curve, this is an M 1.5 level flare, shown in Figure 9. A flare occurred in the active area NOAA12929 (N07W56). The National Oceanic and Atmospheric Administration (NOAA) observed the complete process of the flare, while the Solar Terrestrial Relations Observatory (STEREO/A) could only view the flare from the "rear," resulting in only images of the evolution of the flare in the upper atmosphere. SOHO/LASCO C2 observed a northwestern coronal mass ejection (CME) more than half an hour after the flare, and STEREO/SECCHI COR2 observed it almost simultaneously.

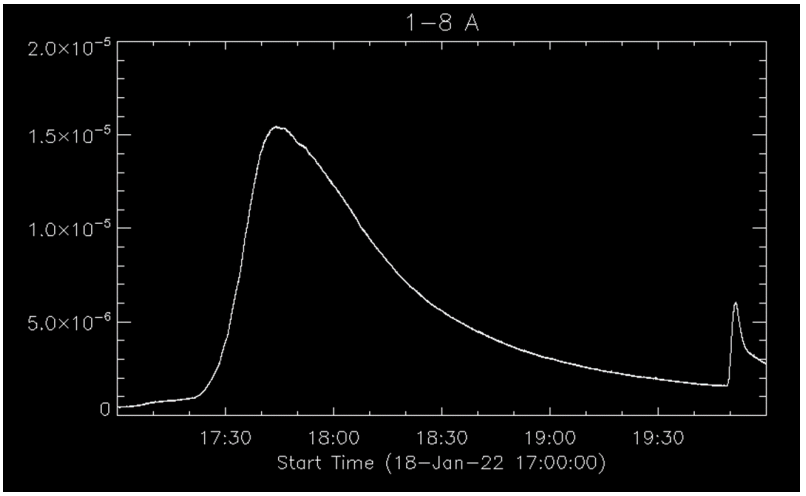


**Figure 9. Flow curve of GOES satellite 1-8**

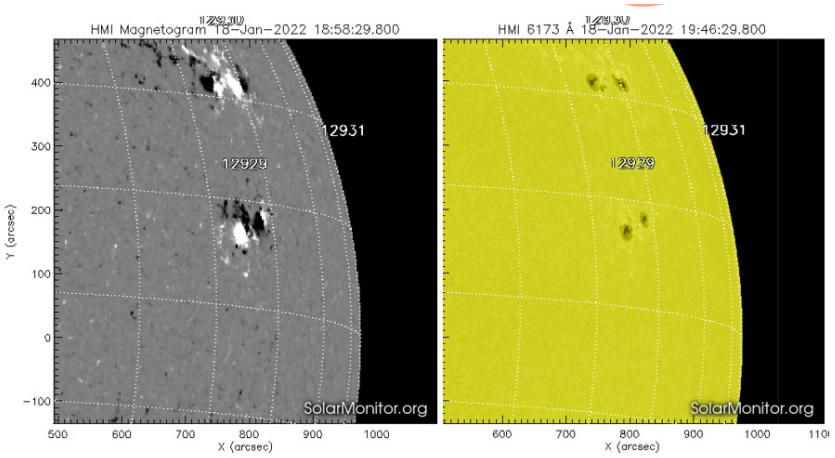


**Figure 10. Local visible magnetic map of the day; right: Local visible light map of the day**

The active zone of the flare burst is primarily characterized by a complex β γ β-shaped quadrupolar magnetic field structure, comprising two prominent black spots. The flare burst commenced at 17:20 UT, reached its maximum intensity at 17:44 UT, and subsequently entered the attenuation phase.

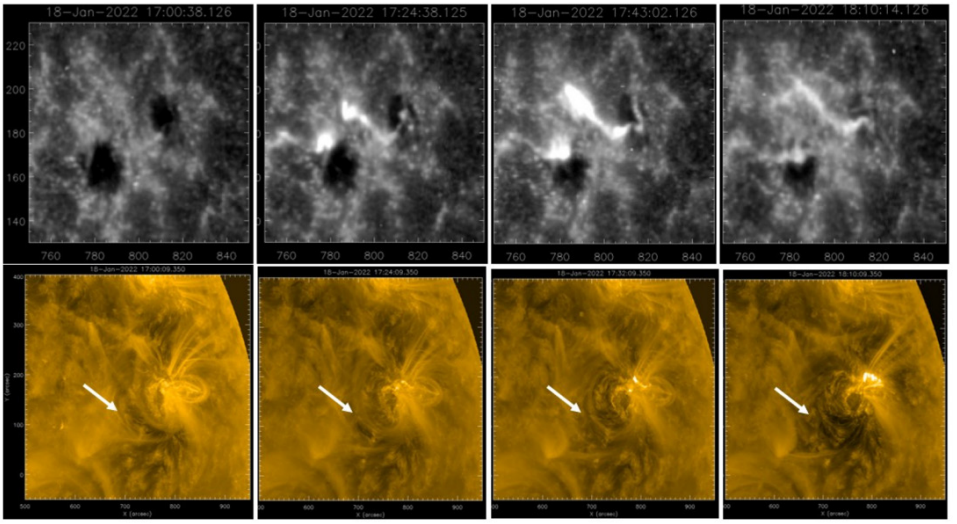


**Figure 11. The SDO/AIA multiband plot. Upper row: 1600A; lower row: 171 A.**

ISSN 2959-6157

Figure 11 shows a multi-band observed image of this flare. The SDO/AIA 1600A image shows that this is a typical two-band flare. At 17:02 UT there is a bright spot between two large spots. Soon a bright extension appears in the upper right bright spot through the shadow of the black spot, and in the left shadow of the black spot above the bright spot. Then a larger bright spot appears in the upper left of the right bright band and soon forms a large bright band with the original two right bands. At the same time, the left bright spots also brightened rapidly, but the shape did not change significantly.. The two bright bands peaked at 17:30 UT, lasted for about 10 minutes, and then faded. There is no significant change in the distance between the two bright bands.

The flare shows a different evolution in the EUV band. The SDO/AIA 171A images show that the evolution of the EUV bright band after the flare burst is similar to that of 1600A, but a distinct post-flare loop forms between the two bright bands after the pulse phase. Interestingly, after the flare burst, the EUV ring outside the active zone marks the generation of EUV waves centered on the flare (shown in Figure 11, white arrow). From the continuous image of SDO/HMI we can see that the two large black spots did not change significantly before and after the flare outburst. Interestingly, there is a penumbra-like structure in the middle of the two spots before the flare, marking the position of a magnetic flux under the photosphere. According to the SDO/HMI L OS magnetic field map, this is a weak bipolar magnetic field dominated by negative polarity. Over time, this regional scale increases and deepens before the flare bursts, indicating that the hidden magnetic field below is changing and emerging from beneath the photosphere.

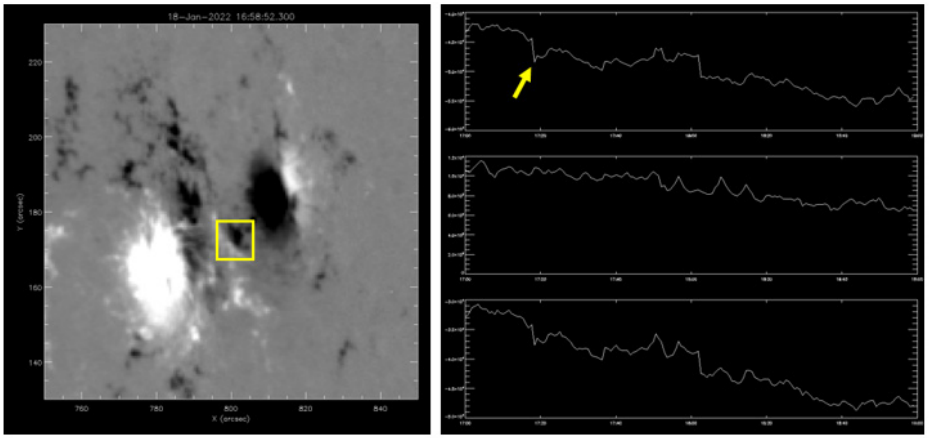


**Figure 12. Left figure SDO/HMI visual magnetic field map, box for calculating the magnetic flow area, right figure top: negative magnetic flow curve, middle positive magnetic flow curve, bottom total magnetic flow curve.**

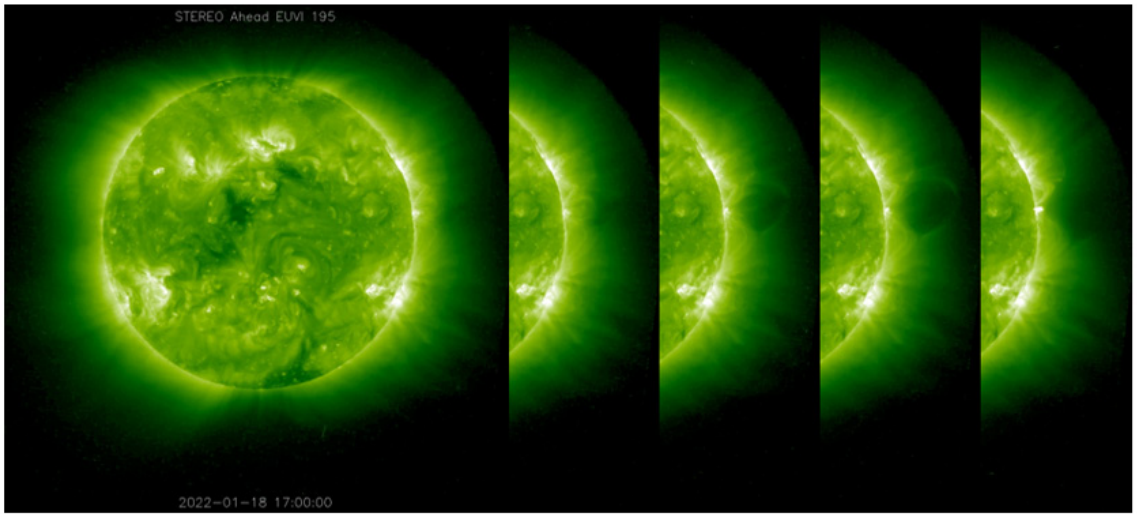


**Figure 13. STEREO/A 195A image. The SCEHHI/CRO2 of STEREO/A was observed for the first time at 17:53 UT.**

As illustrated in Figure 12, the STEREO/A satellite was situated on the left side of the Earth at that specific point in time. The angle between the Earth and the perspective view was approximately 34.7 degrees, which resulted in the active area 12929 being occluded and precluded observation of the initial stages of the flare. 5. However, the STEREO/A far UV 195A image (Figure 13) reveals the presence of a pointed structure exhibiting continuous upward movement at the northwest edge. This structure corresponds to the tip of the posterior ring structure, as observed in the far UV band of 171A. Of particular interest is the observation of a bubble-shaped structure situated directly above the bright spire structure at 17:10 UT. This structure exhibited a rapid outward expansion as the tip moved upward at a velocity of approximately 150 km/s. At 17:35 UT, the front edge of the bubble structure departed from the observable range of STEREO/A in band 195A.

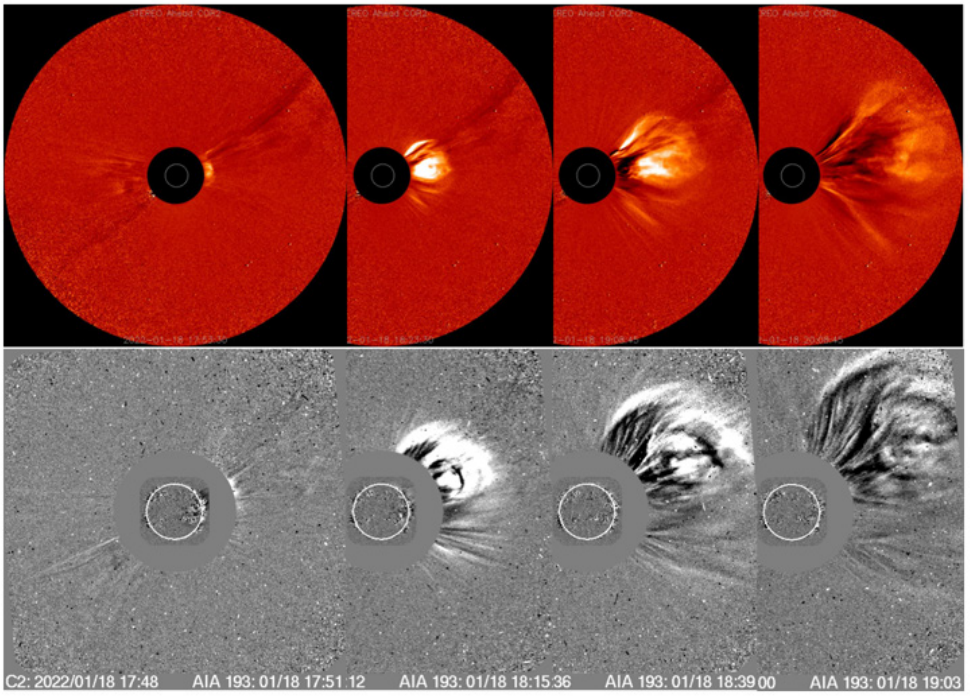


**Figure 14. The plot of CME evolution observed by STEREO/SECHHI (a) and SOHO/LASCO (b)**

The CME possessed an angular width of about 100 degrees and had a typical three-component structure (Figure 14). We observed a bubble-like structure expanding into interplanetary space, and it is likely that the 195A band produced a CME. The SOHO satellite LASCO/C2, from 17:48 UT, observed a northwest CME on the northwest edge of the day and erupted rapidly.

ISSN 2959-6157

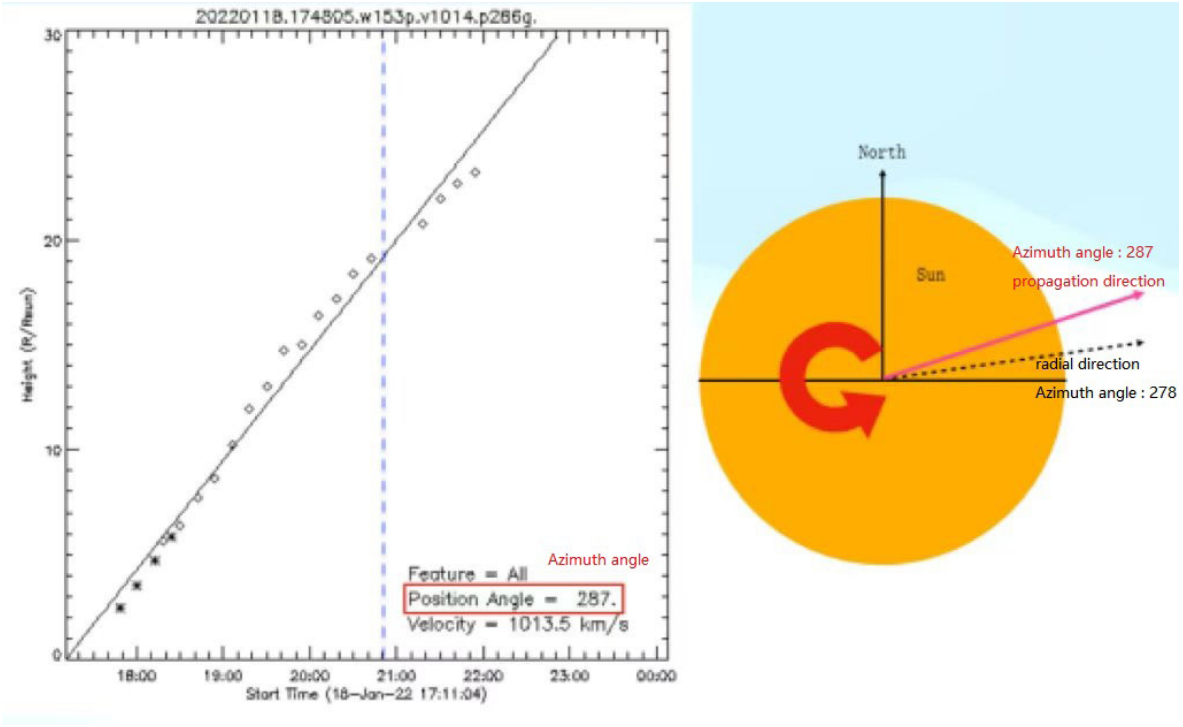


**Figure 15. Left figure: CME parameters calculated by improved cone simulation, right figure: simulated CME space pointing**

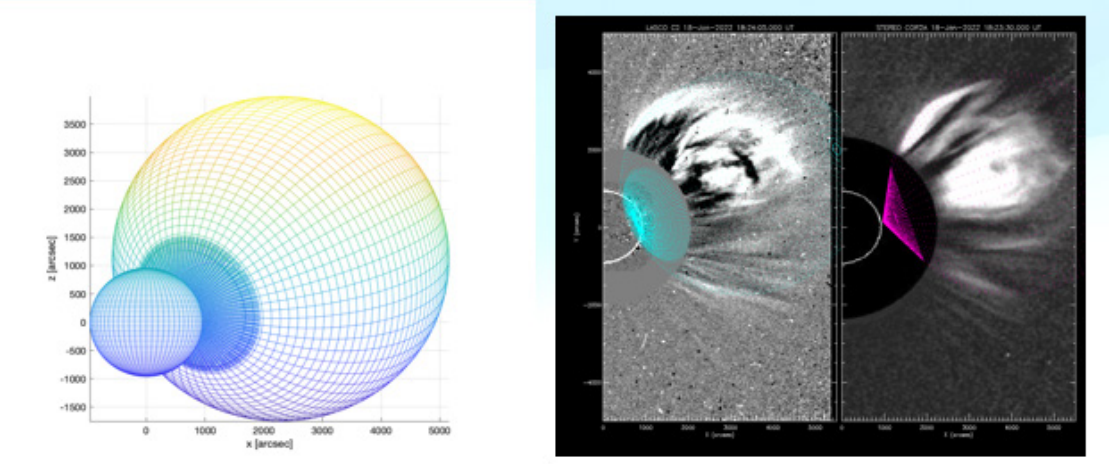

**Figure 16. Left figure: The CME morphology simulated by the modified cone model, the left small ball is the sun, and the large ball is the simulated CME. Right: Superimposing the simulated CME 3D structure onto the coronagraph observation image.**

Compared to observations of STEREO and SOHO, we suggest that SECHHI/CRO2 and LASCO/C2 observe projections of the same CME in different perspectives. As shown in Figure 15, using the observation of LASCO/C2, it is known that this CME eruption is on the northwest edge of the sun, and the azimuth angle of the relative solar sphere center is 287 degrees and the projection velocity is 1013.5km/s.

Using the improved cone model to simulate the spatial three-dimensional evolution of this CME will help us to understand this CME outbreak. Based on the observations of SECHHI/CRO2 and LASCO/C2, combined with the position relationship between S TEREO/A and SOHO, the modified cone model calculated the azimuth of 278 degrees and the true speed of 1409 km/s, and the 3D structure of CME was obtained (Figure 16).

## 4 Results and discussion

Multi-band analysis of a flare and CMM event was conducted on January 18, 2022.The SDO/AIA observations show that this flare is a typical two-band flare. The flare burst in the active region 12929 is triggered by the emergence of two large black ones with opposite polarity. Using the LOS magnetic map of SDO/HMI, negative polar currents emerge in the region and disappeared with the positive current before the flare. Flare outbreak early, the EUV/UV band shows two obvious bright belts, one bright belt with one end through the shadow, and the corresponding another bright belt has been appearing on the outside of the spot, and two bright belts in the whole outbreak process has maintained a fixed relative distance, not like the classic double belt flares double belt will gradually separate.

In the EUV band (e.g. , 171A), distinct flare post-flare rings appear between the two bright bands. At the same time, the flare also causes EUV waves, which drive the expansion of the EUV ring and push away the EUV ring (magnetic field) covered by the upper layer.

From the perspective of the active area, the evolution of the flare in the low atmosphere is not observable; only the tip structure of the ring is discernible following the flare. It is noteworthy that following the flare event, the EUV ring situated above the active region exhibits a gradual outward expansion. The analysis demonstrates that the expansion of the EUV ring is consistent with the expansion of the ring observed by SDO/AIA. As the flare progressed, STEREO observed the formation of a bubble-like structure above the flare. This bubble expanded rapidly near the peak, after which it fully opened, indicating the occurrence of a coronal mass ejection. The expansion rate of the bubble structure was observed to be approximately 200 km/s throughout the entire process.At 10 minutes after the flare peak (approximately 17:50 UT), SOHO/LASCO and STEREO/SECHHI both detected a northwest-facing CME. Considering the observed azimuth and angular width of STEREO/SECHHI, we believe that these two are plane projections of the same CME at different angles.

A “black box” of 1/2 solar radius exists between the observed fields of the coronagraph and SDO, which precludes further analysis. The occluded area precludes an accurate assessment of the source region of the CME. However, based on the correlation between morphological evolution and time evolution, it can be postulated that the flare and CME represent two distinct manifestations of a single eruption. The eruption initially triggers the flare and displaces the magnetic field above the active region. The accelerated high-energy particle flow then propels through the disrupted magnetic field gap, forming the CME.Based on the position relation and observational data of STEREO/A and SOHO, the 3D simulation of this CME using the modified cone model gives an orientation angle of 278 degrees and a velocity of 1409km/s. Considering the eruption direction and speed of this CME, we judged that there would be no destructive impact on the earth. By querying the geomagnetic storm data of the following days, it was also confirmed that there was no change in the earth’s magnetic field.

The results of the simulation demonstrate that the availability of more comprehensive and precise observations of coronal mass ejections (CMEs) will significantly enhance the utility of three-dimensional reconstruction methods for forecasting the impact of CMEs on interplanetary and Earth space environments.

## 5 Closing remark and Future Research

The instruments on board the satellite permit uninterrupted observations of the early evolution of the CME with high temporal and spatial resolution, thereby offering considerable optimism that the trigger problem will be resolved within the solar cycle. A multitude of space-based and ground-based observatories, including SOHO, STERO, Hinode, SDO, GOES, REHHSI, and others, will facilitate observations of unprecedented quality. The diverse observational advantages will facilitate a more profound comprehension of the multifaceted activity phenomena on the Sun, which will ultimately establish a robust foundation for precise space weather forecasting.

## References

1. SOHO LASCO CME CATALOG - CDAW DATA CENTER. (n.d.). https://cdaw.gsfc.nasa.gov/CME_list/

2. Lemen, J. R., Title, A. M., Akin, D. J., Boerner, P. F., Chou, C., Drake, J. F., ... & Waltham, N. (2012). The atmospheric imaging assembly (AIA) on the solar dynamics observatory (SDO). Solar Physics, 275, 17-40.

3. Scherrer, P. H., Schou, J., Bush, R. I., Kosovichev, A. G., Bogart, R. S., Hoeksema, J. T., Liu, Y., Duvall, T. L., Zhao, J., Title, A. M., Schrijver, C. J., Tarbell, T. D., & Tomczyk, S. (2011). The Helioseismic and Magnetic Imager (HMI) investigation for the Solar Dynamics Observatory (SDO). Solar Physics, 275(1–2), 207–227.

4. Brueckner, G. E., Howard, R. A., Koomen, M. J., Korendyke, C. M., Michels, D. J., Moses, J. D., Socker, D. G., Dere, K. P., Lamy, P. L., Llebaria, A., Bout, M. V., Schwenn, R., Simnett, G. M., Bedford, D. K., & Eyles, C. J. (1995b). The Large Angle Spectroscopic Coronagraph (LASCO). Solar Physics, 162(1–2), 357–402.

5. Howard, R. A., Moses, J. D., Vourlidas, A., Newmark, J.

ISSN 2959-6157

S., Socker, D. G., Plunkett, S. P., Korendyke, C. M., Cook, J. W., Hurley, A., Davila, J. M., Thompson, W. T., St Cyr, O. C., Mentzell, E., Mehalick, K., Lemen, J. R., Wuelser, J. P., Duncan, D. W., Tarbell, T. D., Wolfson, C. J., . Carter, T. (2008). Sun Earth Connection Coronal and Heliospheric Investigation (SECCHI). Space Science Reviews, 136(1–4).

6. Michałek, G., Gopalswamy, N., & Yashiro, S. (2003). A new method for estimating widths, velocities, and source location of halo coronal mass ejections. The Astrophysical Journal, 584(1), 472.

7. **e, H., Ofman, L., & Lawrence, G. (2004). Cone model for halo CMEs: Application to space weather forecasting. Journal of Geophysical Research: Space Physics, 109(A3).

8. Xue, X. H., Wang, C. B., & Dou, X. K. (2005). An ice-cream cone model for coronal mass ejections. Journal of Geophysical Research: Space Physics, 110(A8).

9. Zhao, X. P., Plunkett, S. P., & Liu, W. (2002). Determination of geometrical and kinematical properties of halo coronal mass ejections using the cone model. Journal of Geophysical Research: Space Physics, 107(A8), SSH-13.

10. Zhang, J., Dere, K. P., Howard, R. A., Kundu, M. R., & White, S. M. (2001). On the temporal relationship between coronal mass ejections and flares. The Astrophysical Journal, 559(1), 452.

11. Feng, L., Inhester, B., Wei, Y., Gan, W. Q., Zhang, T. L., & Wang, M. Y. (2012). Morphological evolution of a three-dimensional coronal mass ejection cloud reconstructed from three viewpoints. The Astrophysical Journal, 751(1), 18.

12. L. Fenget al. “A Study on the Magnetic Field and Plasma Parameters of Coronal Mass Ejections at 1 AU” In: Research in Astronomy and Astrophysics 19 (2019), p. 162.

13. Fang Cheng, Ding Mingde, and Chen Pengfei. Solar Zone Physics. Nanjing University Press, 2008